Int J Adv Manuf Technol (2017) 93:3517–3530
DOI 10.1007/s00170-017-0734-y

ORIGINAL ARTICLE

# The characteristics and reduction of porosity in high-power laser welds of thick AISI 304 plate

**Junhao Sun [1,2] · Pulin Nie [1,2] · Fenggui Lu [1,2] · Jian Huang [1,2] · Kai Feng [1,2] · Zhuguo Li [1,2] · Baochao Guo [3] · En Jiang [3] · Wang Zhang [4]**

Received: 6 February 2017 / Accepted: 26 June 2017 / Published online: 21 July 2017


**Abstract** The porosity produced in the 304 stainless steel laser welds was investigated. The laser welding process was conducted at a laser power of 10 kW. Different welding speeds and shielding gases were used. The porosity in the welds was characterized. The welding processes were observed using a high-speed video camera. The mechanism of the elimination of the porosity was revealed. The suppression of the porosity was made in $N_2$ rather than Ar or He shielding gases. The porosity was mainly produced at the root and most of the porosity was less than 0.02 $mm^3$. No significant differences of the metallic plume, liquid melt pool, and laser keyhole were found when Ar or $N_2$ shielding gas was employed. The solubility of $N_2$ in the liquid melt pool contributed to the reduction or elimination of the porosity in the 304-L laser welds.

**Keywords** High-power laser welding · High-speed video camera · Porosity · Shielding gases · Stainless steel

✉ Pulin Nie
nplhxy@sjtu.edu.cn

✉ Kai Feng
fengkai@sjtu.edu.cn

✉ Zhuguo Li
lizg@sjtu.edu.cn

[1] Shanghai Key Laboratory of Materials Laser Processing and Modification, School of Materials Science and Engineering, Shanghai Jiao Tong University, Shanghai 200240, China

[2] Collaborative Innovation Center for Advanced Ship and Deep-Sea Exploration, Shanghai 200240, China

[3] Shanghai No. 1 Machine Tool Works Co., Ltd, Shanghai 201308, China

[4] Air Liquide (China) R&D Co., Ltd, Shanghai 200233, China

## 1 Introduction

Thick section material welding has been widely used in shipbuilding, power plants, high-speed trains, and oil/gas transportation pipe lines. Traditional methods like arc welding or plasma welding were difficult to join the thick plate because the rather high-heat input could lead to large welding distortion [1, 2]. Recently, high-power laser welding has received more and more attention as a promising technology in joining of thick plate due to their advantages in high energy density, low heat input, large depth-to-width ratio, narrow heat-affected-zone, and minimal distortion. Moreover, laser welding can be conveniently automated with robots, which could offer more flexible beam delivery [3].

The porosity might produce in the laser weld, which could have detrimental effects on the fatigue resistance of a component. The porosity is considered as a competitive weld imperfection, because it is the site of crack initiation and decreases the fatigue strength of the weld joint [4]. It is necessary to study the porosity formation in laser welding and find a way to decrease or eliminate porosity.

A thin capillary is generated during the high-power laser welding process. According to S. Tsukamoto [5] and Ola [6], the keyhole was very unstable. The shape and depth of the keyhole fluctuated all the time, and a bubble was easily formed at the bottom of the molten pool. If the bubble was stopped by the solidified metal, the porosity would be retained. Matsunaga et al. [7] observed the keyhole variation and the molten pool flow using high-speed X-radiography, and depression at the back wall of the keyhole gave rise to bubble. Kawahito et al. [8] found that pores were formed at the tip and the middle of the keyhole. Zhao et al. [9] established a model to describe the keyhole fluctuation of laser welding. The results showed that the keyhole depth self-fluctuated

continuously, and the bubbles formed from keyhole collapse, and shrinkage was the cause of keyhole-induced porosity.

Many techniques have been proposed to reduce the porosity in the laser welds. Kuo et al. [10] investigated the influence of the laser power wave mode on the porosity of weldments. The square wave power modulation at the eigenfrequency of the molten pool oscillation was effective in decreasing the porosity due to the stabilization of the keyhole perturbation. Beretta et al. [4] showed that it was effective to substitute He with $N_2$ as a shielding gas in laser welding of aluminum alloys. The keyhole behavior was similar to that of pulsed wave laser welding where porosity was strongly reduced in $N_2$. Harooni et al. [11] studied the pore formation mechanism and its mitigation in laser welding of AZ31B magnesium alloy and revealed that the preheating procedure could effectively mitigate pore formation. Kamimuki et al. [12] found that side-blowing gas could compress the surface of the molten pool, making the molten pool wider and keyhole more stable, thus reducing the porosity in weld. Meng et al. [13, 14] observed the keyhole and molten pool dynamic behavior in laser lap welding T-joints, and found that porosity was suppressed by maintaining a small gap or adopting high welding speed.

According to [10–14], though there were methods such as the use of wave laser power, preheating procedure, different welding configuration, and various welding parameters, they only reduced the porosity diameter and volume to a certain degree, and it was difficult to eliminate the porosity entirely. In addition, most studies were focused on the porosity produced in the thin plate with relatively lower laser power, and the porosity formed in the thick plate was insufficient. Thus, this study investigated the porosity formed in the thick plate with high power laser welding. Different shielding gases were tried in order to totally suppress the porosity. It was mentioned that $N_2$ contributed to the suppression of porosity produced in laser welding of 304 plates [7], but the explanation of this phenomena was lacking. So, the mechanism was analyzed and discussed in detail. Moreover, the characteristics of the porosity, which included the shape, the size, and the volume, were observed and counted carefully under each welding parameter, and this was not investigated based on previous studies. Eventually, the thick 304 plates were successfully welded and sound joint with good appearance and no porosity was achieved.

## 2 Materials and experimental procedures

The 304 austentic stainless steel was chosen in this study, and the plates used in the experiment were 16 and 20 mm in thickness. The chemical composition of the base metal is listed in Table 1. The microstructure of the as-received material is presented in Fig. 1. The microstructure shows an exquiaxed and twinned austenite, and the alignment of δ-ferrite precipitates indicates the rolling direction.

**Table 1** Nominal chemical compositions of AISI 304

| Alloys | Elements/wt.% | | | | | | | |
|---|---|---|---|---|---|---|---|---|
| | Fe | C | Mn | Si | S | P | Cr | Ni |
| AISI 304 | Bal. | 0.027 | 1.6 | 0.36 | 0.002 | 0.01 | 18.5 | 11.6 |

The welding setup is shown in Fig. 2. As seen in Fig. 2a, the laser welding process was conducted in a horizontal butt joint configuration. According to previous results, a U-shaped groove fabricated on the thick plate could greatly increase the weld penetration and decrease the weld width. A groove that had a depth of 2 mm and a width of 4 mm was optimized for the 16-mm plate [15]. A large amount of porosity was found in the laser welds. Further works were done to reduce the porosity. A continuous wave IPG fiber laser (IPG YLS-10000) operating at 1.070 ± 0.010 mm wavelength was used to perform the laser welding, and the beam shape used in this study is shown in Fig. 2b. For the power levels used in this study, the beam had a beam parameter product of 12.5 mm mrad and a rayleigh length of 10.328 mm. At sharp focus, the minimum beam diameter was measured to be 0.72 mm. The beam was optically delivered with the output lenses held in the welding head mounted on a KUKA 6-axis's robot.

The laser beam was tilted 10° toward the front of the weld pool in order to protect it from the back reflection of the light. The laser was focused on the groove surface of the sample, and a laser power of 10 kW was used. The welding speeds varied between 0.8 and 3.0 m/min. A plasma suppression gas nozzle with an 8-mm diameter orifice was directed at the beam impingement point at a 45° angle with a flow rate of 15 L/min, and a trailing gas diffuser with a flow rate of 20 L/min was used to minimize oxidation of the weld. Different gases were chosen for this study, which included inert gases of Ar and He and reactive gas of $N_2$. The mixed gases of Ar + $N_2$, which include 100% Ar, 80%Ar + 20%$N_2$, 60%Ar + 40%$N_2$, 40%Ar + 60%$N_2$, 20%Ar + 80%$N_2$, and 100% Ar, were also used as the shielding gases to further analyze the influence of $N_2$ on the reduction of porosity that formed in the laser welds of 304L.

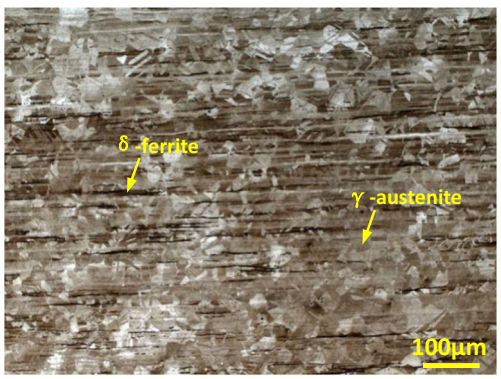


**Fig. 1** Microstructure of base metal of AISI 304 stainless steel plate

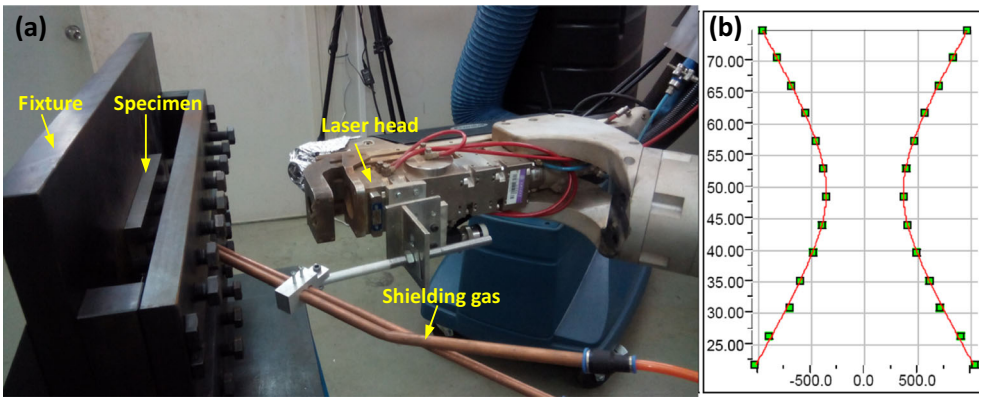


**Fig. 2** The laser welding setup in a horizontal butt joint configuration. **a** The welding process. **b** The beam shape

The welding processes, including the dynamics of the weld pool, the laser keyhole, and the vapor plume, were observed by a standard CMOS high-speed video camera (Photron Fastcam SA4). The welding process was recorded at a speed of 4000 frames per second. When the weld pool and keyhole were observed, a low-power laser-assisted light (Cavilux) with a wavelength of 810 nm was used as an illumination source to illuminate the welding zone. A narrow band-pass interference filter was placed in front of the camera lens to block scattered light. When the vapor plume was observed, the laser-assisted light and the interference filter were not used. The experimental setup is shown in Fig. 3.

The coupons were radiographed to film to observe porosity. The radiograph shown in Fig. 4 presents the laser weld that was obtained with a laser power of 10 kW, a weld speed of 0.8 m/min, and a shielding gas of Ar. The weld made in Ar had substantial porosity that was mainly located at the center of the weld. The samples of the cross-section and longitude-section were cut using the wire-electrode method to observe the porosity distribution. The cutting process of the longitude section is shown in Fig. 5a. After the longitude section of the sample (i.e., Fig. 5b) was obtained, the porosity in the laser welds was observed by optical microscopy. The dimensions of the porosity, including the minimum diameter $D_{min}$, the maximum diameter $D_{max}$, and the mean diameter $D_{mean}$, were measured using the software image-pro. Then, the shape of the porosity could be expressed by the ratio of $D_{max}$ to $D_{min}$, and the porosity volume was calculated according to the mean diameter $D_{mean}$. The porosity location was also measured to show the porosity characteristics in the laser welds.

## 3 Results and discussion

### 3.1 Porosity formation in laser welding of a 16-mm 304L plate in 2G position

A 304L stainless steel of 16-mm thickness needed to be welded in a horizontal butt joint configuration. Bead-on-plate welding was performed firstly, but full penetration cannot be achieved using the IPG YLS-10000 fiber laser. Then, a U-shaped groove, which had a width of 4 mm and a depth of 2 mm, was fabricated on the plate. The laser welding process was performed at the center of the groove. Full penetration of the plate was obtained. Figure 6a, b compared the cross-sections of the joints without (i.e., Fig. 6a) and with (i.e., Fig. 6b) the groove, and the penetration increased from 11.52 to 14 mm. Figure 6c, d presents the top and bottom appearance with a U-shaped groove. Sound appearance was produced with no spatter at the top side and no sagging at the back side. However, there was a large amount of macro-porosity in the laser weld, as seen in Fig. 6b. Wei et al. [16] showed that the size distribution and volume fraction of porosity had a significant influence on the mechanical properties

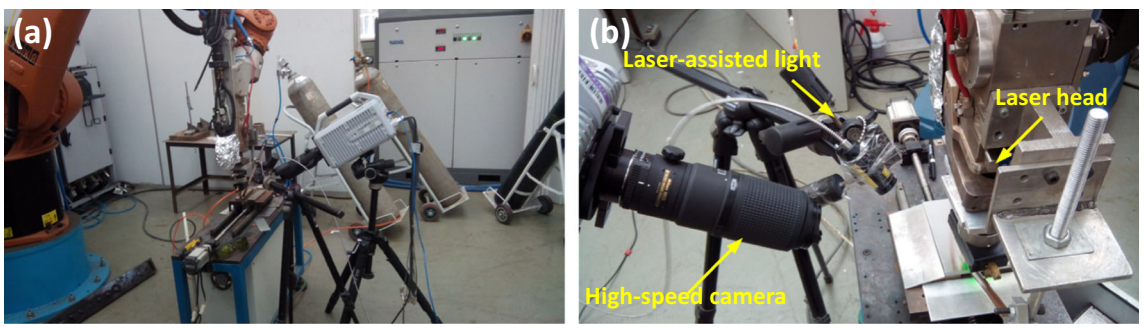


**Fig. 3** The experimental setup for observing the laser welding process with **a** a far visual angle and **b** a close visual angle

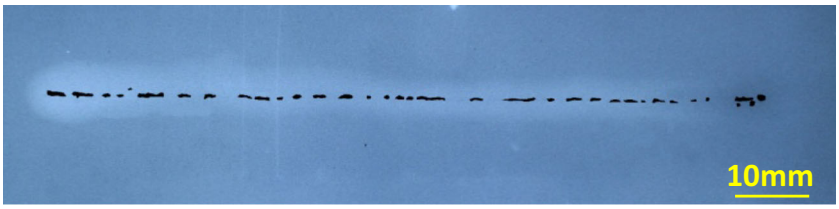


**Fig. 4** Radiograph of laser weld made in 304L stainless steel with a shielding gas of Ar

of welds. Therefore, further experiments were done to study the porosity and find a way to reduce or eliminate the porosity in the welds.

### 3.2 The porosity using different shielding gases and different welding speeds

Experiments were conducted using Ar. Different welding speeds, which varied from 0.6 to 3.0 m/min, were tried with a laser power of 10 kW. The cross and longitude sections were obtained and the results are shown in Figs. 7 and 8.

As seen in Fig. 7, the porosity occurred in all the joints except the last one. The large and irregular porosity was formed at the lower part of the laser welds. The round porosity was formed at the medium and upper part of the welds. Careful examination of the longitude section was done to observe the porosity next.

Figure 8a shows the porosity at the welding speed of 0.6 m/min. In order to observe the porosity clearly and measure the dimension for further analysis, the background color of Fig. 8a was converted through the software, and the result is presented in Fig. 8b. The porosity was produced and retained in all the laser welds in Fig. 8. However, the general quantity and distribution of the porosity was different. As seen in Fig. 8a–d, a large amount of porosity was retained when a welding speed of 0.6–1.5 m/min was used. The porosity was divided into two layers that included the root layer and the upper layer. Most of the porosity was located at the bottom. The apparent periodic nature of the root porosity was found. Many studies showed that keyhole dynamics were playing a key role in the porosity formation. Large amount of porosity was located at the bottom, indicating that the keyhole was mainly collapsed at the lower part. When the welding speed exceeded 2.0 m/min, the porosity was reduced greatly, as seen in Fig. 8e–g. The maximum size of porosity was also reduced with increasing welding speed. Tucker et al. [17] also found that increasing travel speed dramatically reduced porosity in laser welds. Katayama et al. [18] attributed this to the different plume and keyhole behavior under different welding speed. A keyhole collapsed easily and a laser beam was shot on the poured liquid at low welding speed. Vapor was ejected upwards from the keyhole outlet at higher welding speed, which induced melt flow opposite to the case of low welding speed and prevented invasion of shielding gas, leading to the reduced generation of porosity.

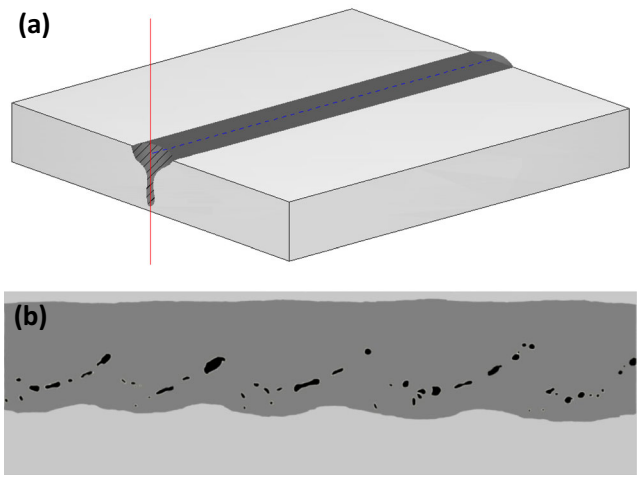


**Fig. 5** The schematic of **a** the segmentation of the laser weld along the center line and **b** the sample of the longitude-section

The shielding gas was also tried to protect the laser weld. The cross and longitude sections, which were produced at welding speeds of 0.6 and 1.5 m/min, are shown in Fig. 9. Severe porosity was still found. However, the distribution of them was different from that was formed using the Ar. Some big and round porosity with great mass occurred in the upper part, whereas only a small quantity of porosity was retained at the root. Therefore, it was difficult to obtain the joint with no porosity using He.

The cross and longitude sections of the laser welds made in $N_2$ are shown in Fig. 10, indicating that no porosity was observed in the cross-sections of the joints. Though some little porosity was found in the longitude-sections, it was acceptable because the effect of this porosity on the mechanical strength could be neglected according to Beretta et al. [4].

### 3.3 Characteristic and quantitative aspect of porosity in laser welds of a 304L plate

Detailed analysis about the characteristic and quantitative aspect of the porosity was conducted. The formation mechanism of the porosity during the laser deep-penetration welding process could be further understood. The shape, location, size, and distribution of the porosity were also learned, which might be helpful for us to determine the performance of the joints.

Large and linear porosity was seen from the radiograph of laser weld, and two layers were observed from the

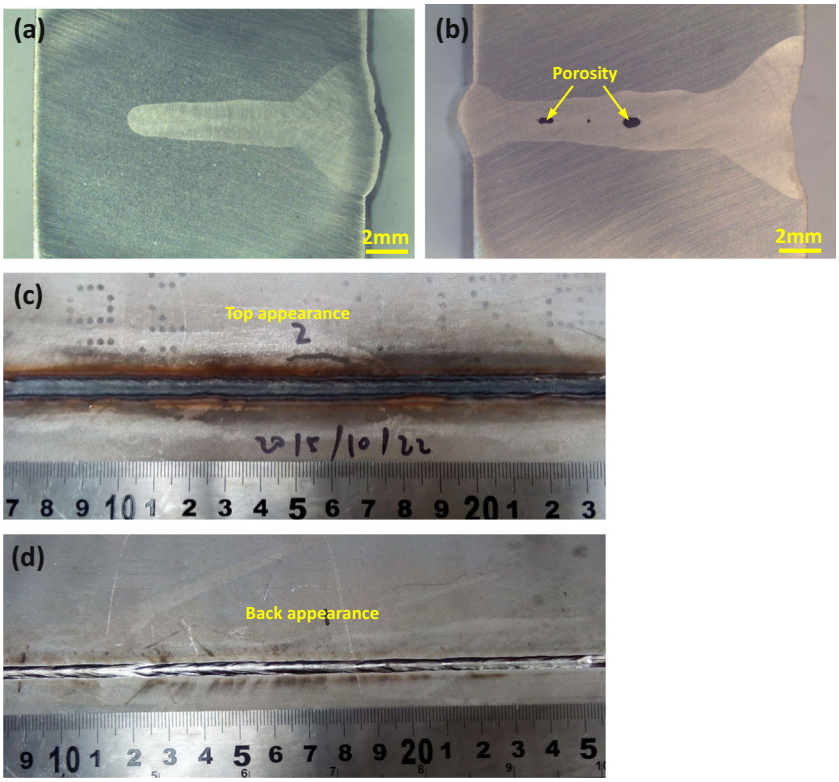


**Fig. 6** The cross-sections of joint **a** without groove and **b** with a U-shaped groove. **c**, **d** Top and bottom appearance with a U-shaped groove

longitude-sections. Careful examination of the porosity was conducted, and the enlargement of the upper and root porosity is shown in Fig. 11. As shown in Fig. 11a, b, the spheroid porosity was formed at the upper laser. The root porosity was irregular. The long and club-shape porosity is presented in Fig. 11c, and the block-shape porosity with intensive distribution is seen in Fig. 11d. In order to find out the shape of all the porosity in the laser welds, the ratio between $D_{max}$ and $D_{min}$ of the porosity was computed, and the results are shown in Fig. 12. When an approximate value of 1 was obtained, the porosity tended to be spherical, while the porosity tended to be irregular with increasing ratio value. As shown in Fig. 12, two layers of porosity were clearly observed. The ratio value was close to be 1 for the upper porosity, and it varied greatly from 1 to 10 for the root porosity. In addition, for the upper

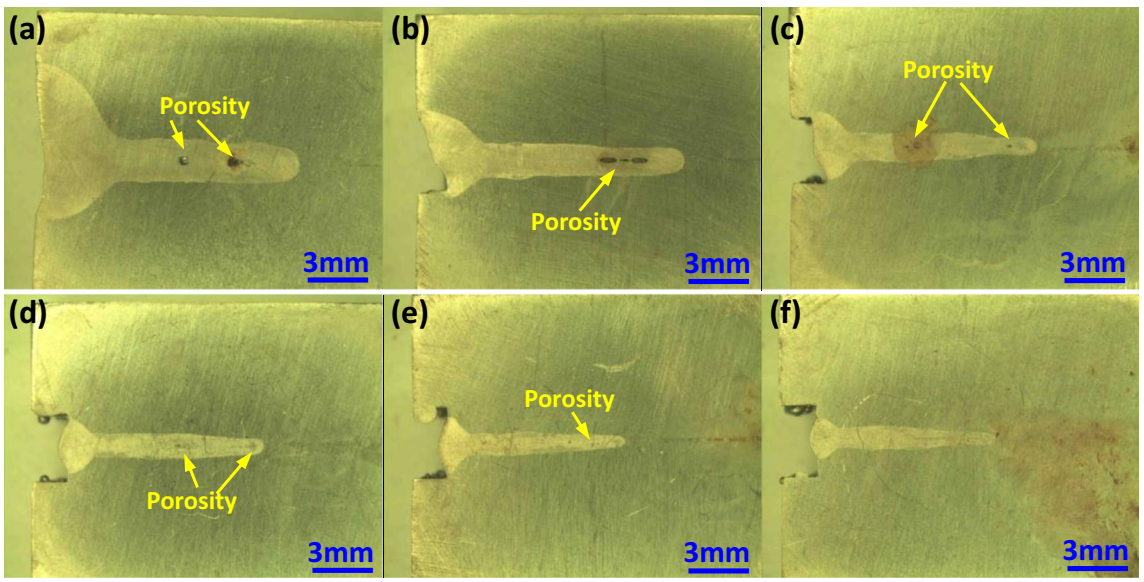


**Fig. 7** The cross-sections obtained with a laser power of 10 kW, a shielding gas of Ar, and different welding speeds of **a** 0.6, **b** 1.0, **c** 1.5, **d** 2.0, **e** 2.5, and (**f**) 3.0 m/min

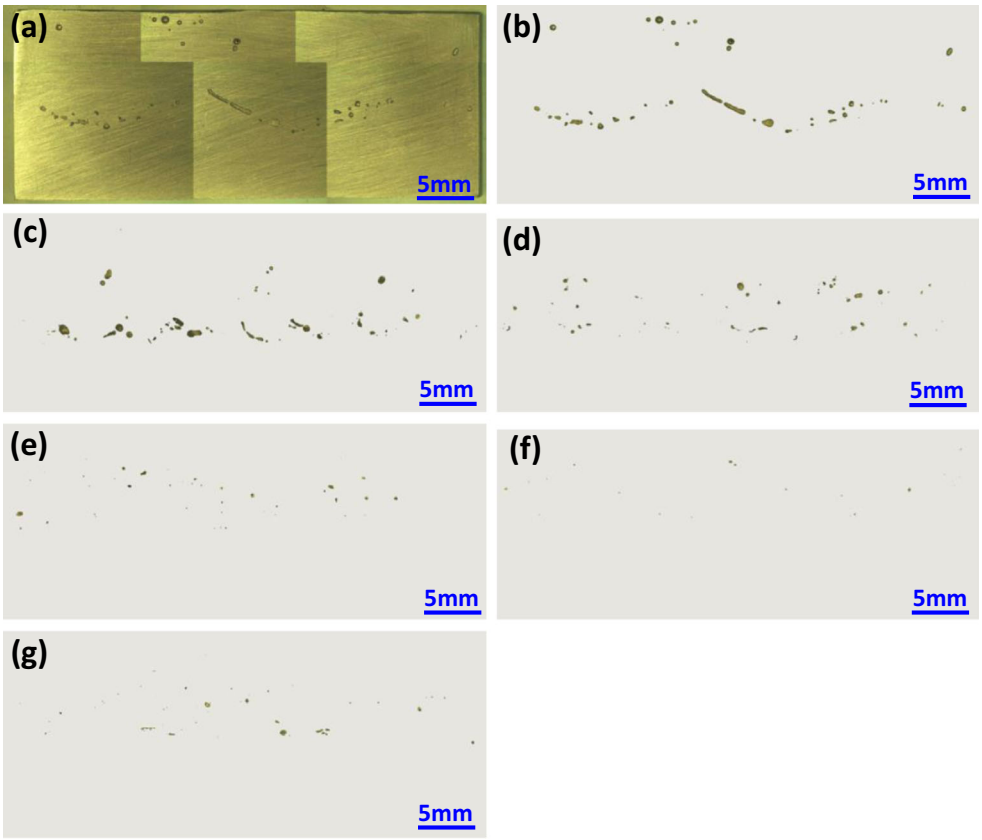


**Fig. 8** The longitude-sections obtained with a laser power of 10 kW, a shielding gas of Ar, and different welding speeds of **a**, **b** 0.6, **c** 1.0, **d** 1.5, **e** 2.0, **f** 2.5, and **g** 3.0 m/min

porosity, the value deviated from 1 with increasing welding speed, as observed in Fig. 12b, d.

A deep keyhole was generated at high intensity values of the laser beam, and the shape and the penetration of the keyhole changed continuously with time. The keyhole was easily collapsed at the tip, and bubbles were produced consequently. Figure 11c, d shows the root porosity, which was produced due to the collapse of the keyhole. In addition, the periodic porosity was observed from Fig. 8a–c, which was caused by the periodic fluctuations and collapse of the keyhole. The production of the spheroid porosity at the upper layer was attributed to the movement of the bubbles during the welding process. Figure 13a, b shows the porosity from the bottom to the upper part of the weld, which indicated the movement tendency of the bubble during the welding process. Moreover, the small bubbles combined and large porosity was retained after welding, as illustrated in Fig. 13c, d. The movement of the bubbles in the weld was attributed to the fast melt flows in the molten pool.

The porosity volume was calculated, and the distribution is shown in Fig. 14. Most of the porosity was less than 0.5 $mm^3$, as seen from Fig. 14. Figure 14a, c compare the porosity volume made in different shielding gases at low welding speed. When Ar was used, the root porosity was bigger than the upper porosity, and the biggest porosity volume was 0.52 $mm^3$. However, when He was used, the root porosity

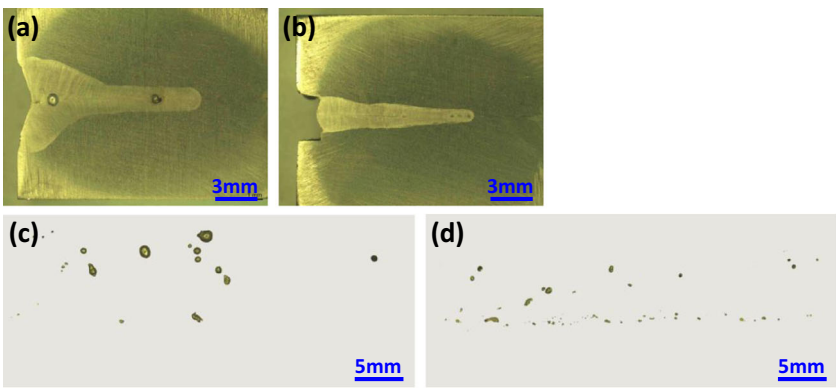


**Fig. 9** The cross-sections and longitude-sections obtained with a laser power of 10 kW, a shielding gas of He, and different welding speeds of **a** 0.6, **b** 1.5, **c** 0.6, and **d** 1.5 m/min

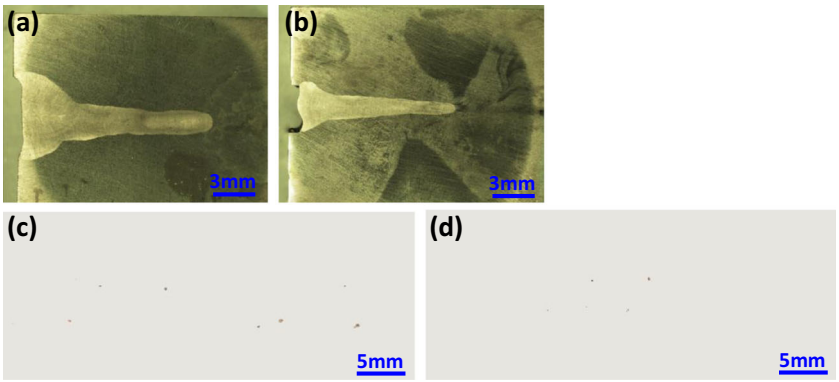


**Fig. 10** The cross-sections and longitude-sections obtained with a laser power of 10 kW, a shielding gas of $N_2$, and different welding speeds of **a** 0.6, **b** 1.5, **c** 0.6, and **d** 1.5 m/min

was smaller than the upper porosity, and the biggest porosity volume was 2.3 $mm^3$. The faster the welding speed was, the smaller the porosity, which can be clearly seen from Fig. 14a, b.

Further analysis was performed to gather statistics on the porosity size distribution, and Fig. 15 plotted histograms of the pore size distribution. All the distributions presented a decreasing frequency with increasing porosity volume, with the largest frequencies occurring at porosity less than 0.02 $mm^3$.

The results were further analyzed to characterize the volume distribution of all the porosity, as shown in Fig. 16. Figure 16a shows the individual porosity volume varying from less than 0.001 up to 2.3 $mm^3$. The volume was less than 1 $mm^3$ for most of the porosity. Smaller range of the porosity volume varying from 0 to 0.6 $mm^3$ is presented in Fig. 16b. As shown, the largest frequency occurred at the smallest volume of less than 0.02 $mm^3$. Figure 16c shows the distribution of the porosity with a volume of less than 0.02 $mm^3$, which also indicated that the largest frequency of porosity occurred at the smallest volume of less than 0.001 $mm^3$. Similar result was also obtained by Elmer et al. [19], and they thought the porosity volume with frequency was described by a Weibull relationship, suggesting the monotonically decreasing function of the frequency with increasing porosity volume. In addition, the very high fraction of small porosity also indicated that the laser welding process produced an abundance of tiny bubbles in the weld pool, which could grow to create the pores before the weld pool solidified and trapped them in the laser weld.

### 3.4 The mechanism of elimination of porosity in 304L laser weld using the $N_2$ shielding gas

According to the above analysis, the welds made in Ar and He had substantial porosity and those made in $N_2$ did not have any observable porosity. Katayama et al. [18] and Pang et al. [20] investigated the gas inside the porosity, and it was revealed that the main gas was the shielding gas. Thus, it could

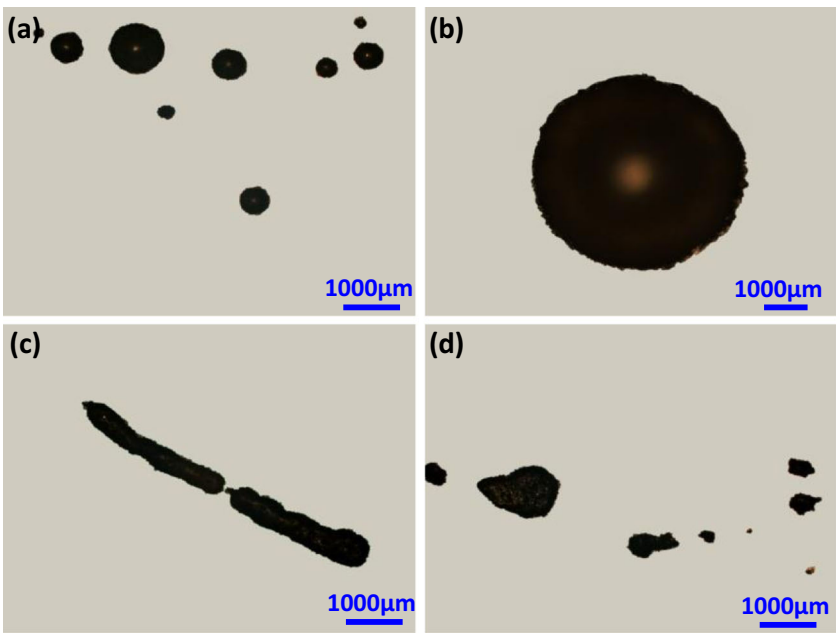


**Fig. 11** The porosity of **a**, **b** the upper layer and **c**, **d** the root layer

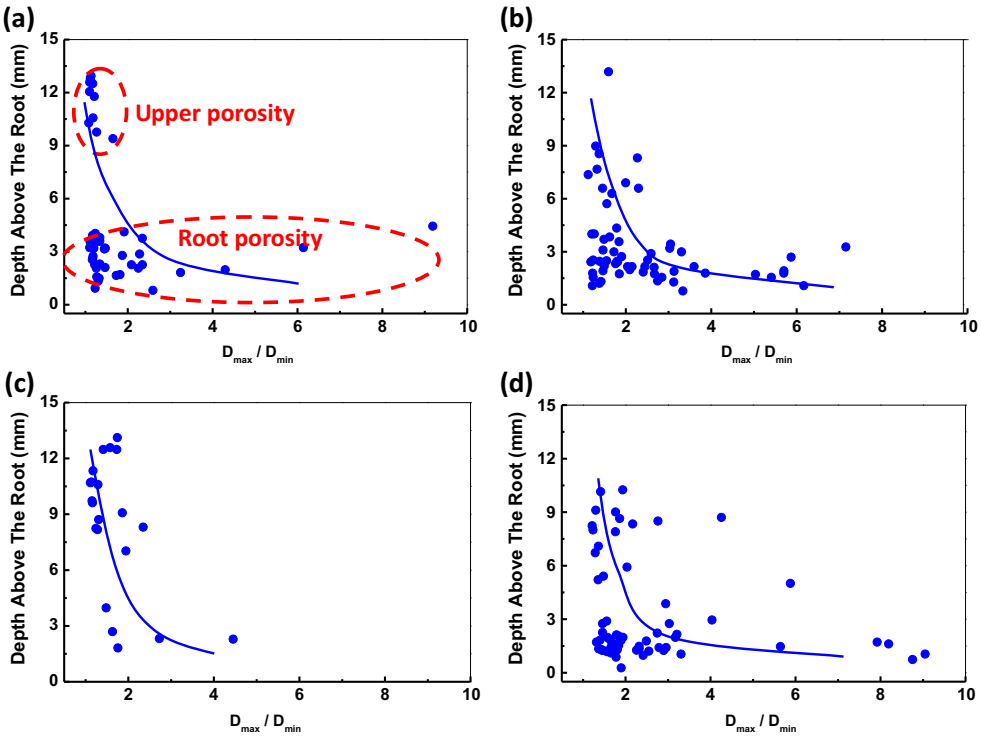


**Fig. 12** The location vs. the ratio between $D_{max}$ and $D_{min}$ of the porosity produced in the laser welds employing different shielding gases and welding speeds of **a** Ar, 0.6 m/min, **b** Ar, 1.0 m/min, **c** He, 0.6 m/min, **d** He, 1.5 m/min

be speculated that the porosity in Fig. 8 was nearly full of Ar, and the porosity in Fig. 9 was nearly full of He.

Two conditions needed to produce the porosity in a laser weld. An unstable keyhole was required to create a bubble in the molten weld pool, and the liquid convection and solidification conditions must be such that the bubble was trapped before it could escape or dissolve into the weld pool.

A high-speed video camera was employed to observe the metallic vapor plume, the melt pool, and keyhole behavior with shielding gases of Ar and $N_2$, and the results are shown in Figs. 17 and 18. Figure 17a–h presented the metallic vapor plume produced with Ar. As seen in Fig. 17a, the metallic vapor ejected from the keyhole under the effect of the direct irradiation of the laser beam, and a bright speck occurred at the inlet at $t_0$. A great mass of bright metallic plume was formed, which expanded and grew very fast, as observed in Fig. 17b, c. The melt pool fluctuated violently, and a cylindrical melt was formed at $t_0$ + 4.5 ms. The cylindrical melt broke and

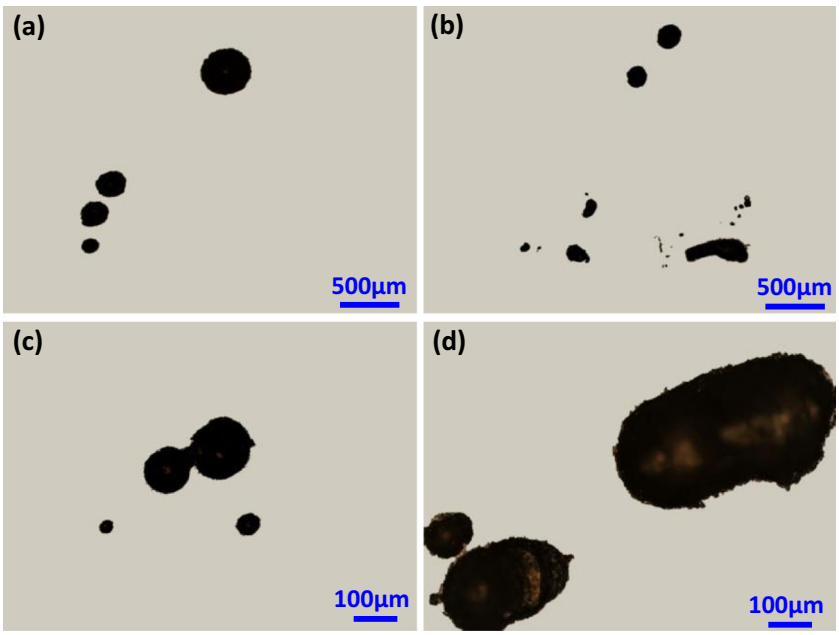


**Fig. 13** The porosity in the welds showing **a**, **b** the moving trend from the bottom to the upper part of the weld and **c**, **d** the combination of the porosity

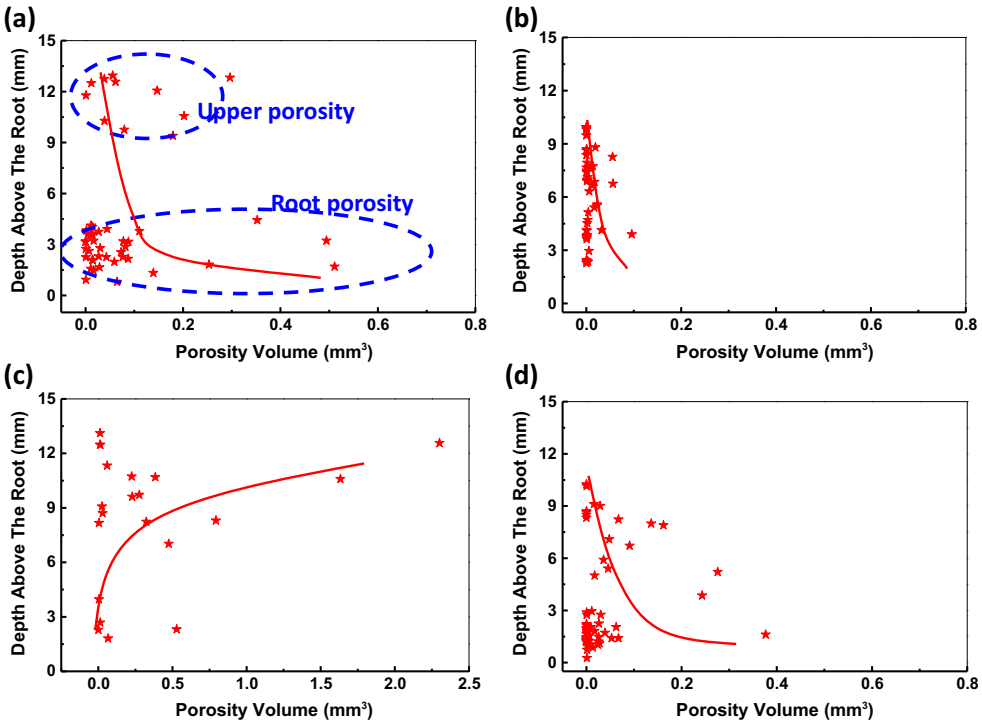


**Fig. 14** The location vs. the porosity volume produced in the laser welds employing different shielding gases and welding speeds of **a** Ar, 0.6 m/min; **b** Ar, 2.0 m/min; **c** He, 0.6 m/min; and **d** He, 1.5 m/min

many spatters were produced at $t_0$ + 7.25 ms. The keyhole collapsed at the same time because the plume started to become thin. Then, the laser beam irradiated into the keyhole again, so the keyhole and the metallic plume varied

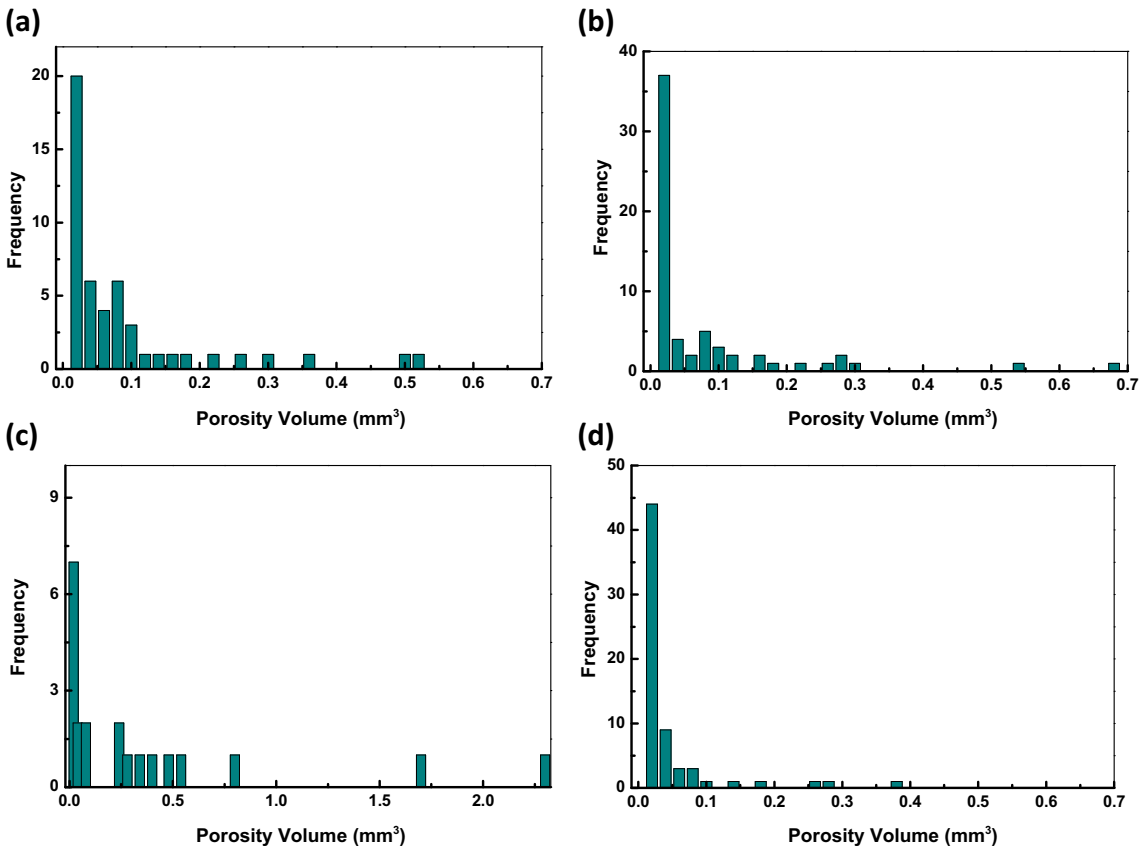


**Fig. 15** The frequency of the porosity volume produced in the laser welds employing different shielding gases and welding speeds of **a** Ar, 0.6 m/min; **b** Ar, 1.0 m/min; **c** He, 0.6 m/min; and **d** He, 1.5 m/min

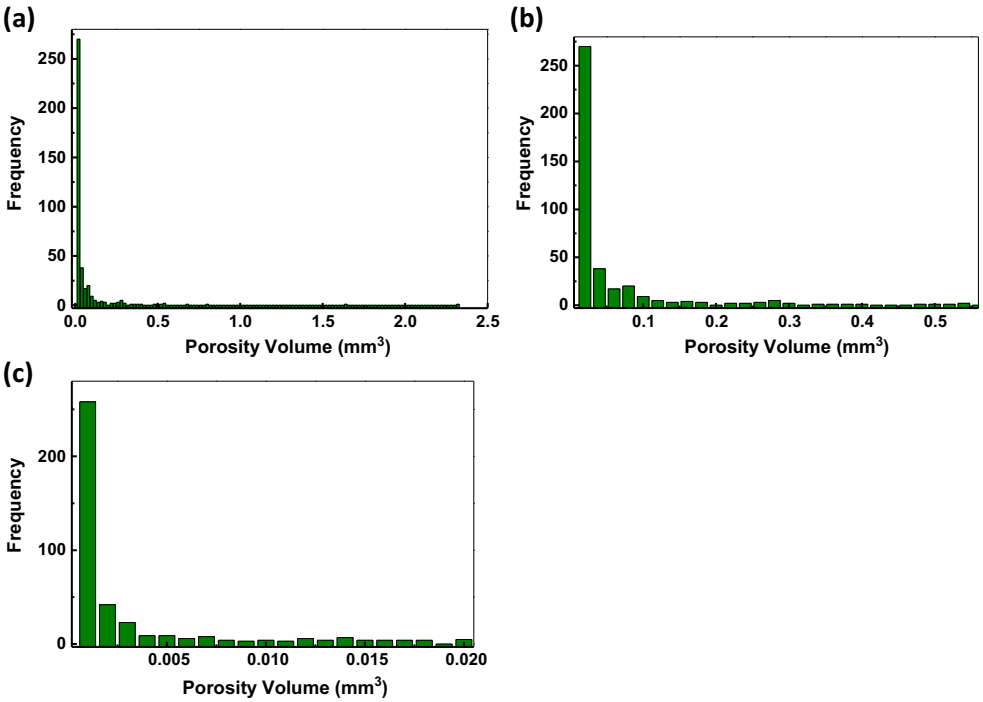


**Fig. 16** The frequency of the overall porosity volume produced in all the laser welds. **a** The distribution for all the pores. **b** The distribution for the pores less than 0.6 $mm^3$. **c** The distribution for the pores less than 0.02 $mm^3$

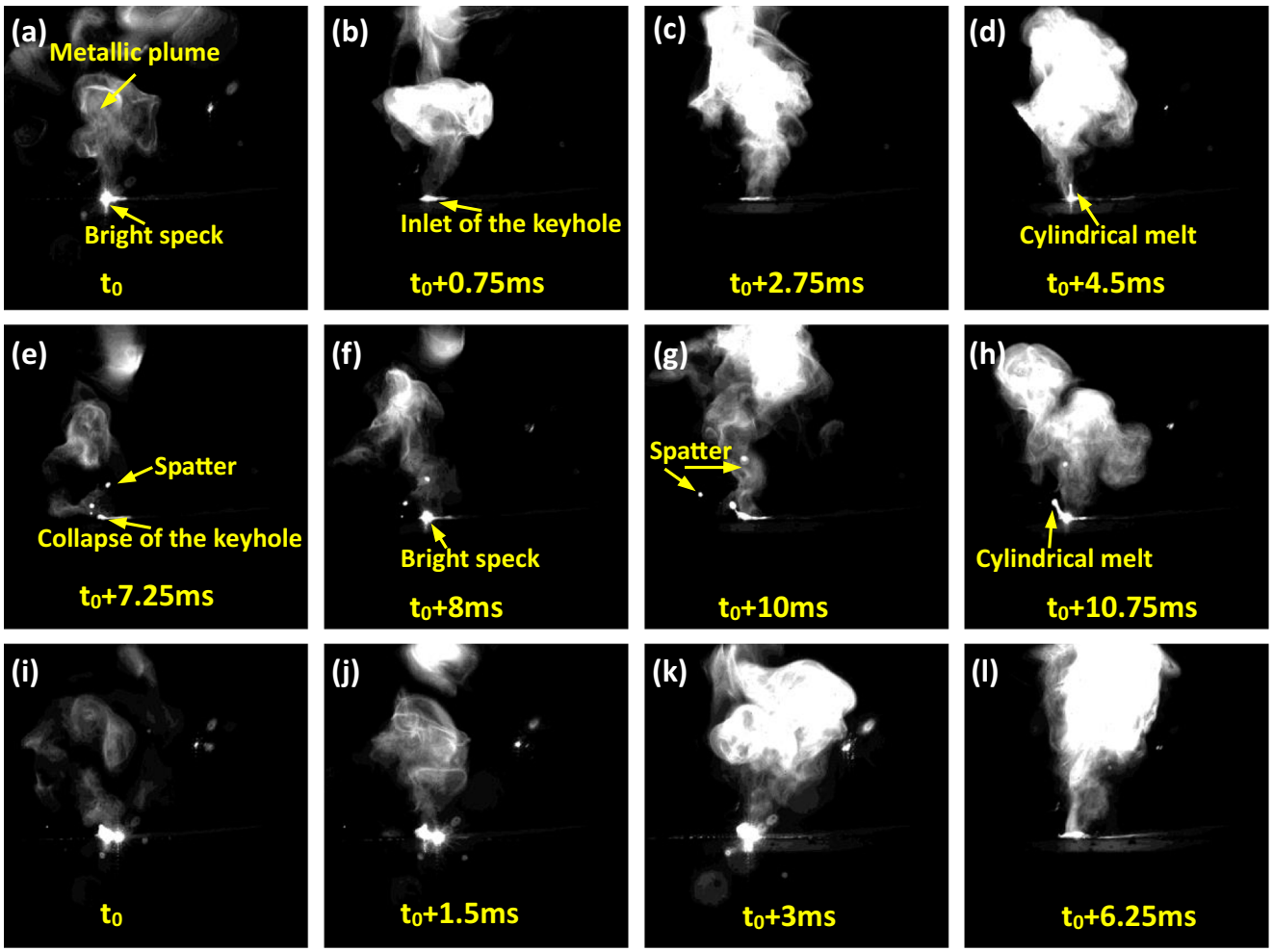


**Fig. 17** The metallic vapor plume behavior using a laser power of 10 kW, a welding speed of 0.8 m/min, and a shielding gas of **a**–**h** Ar and **i**–**l** $N_2$

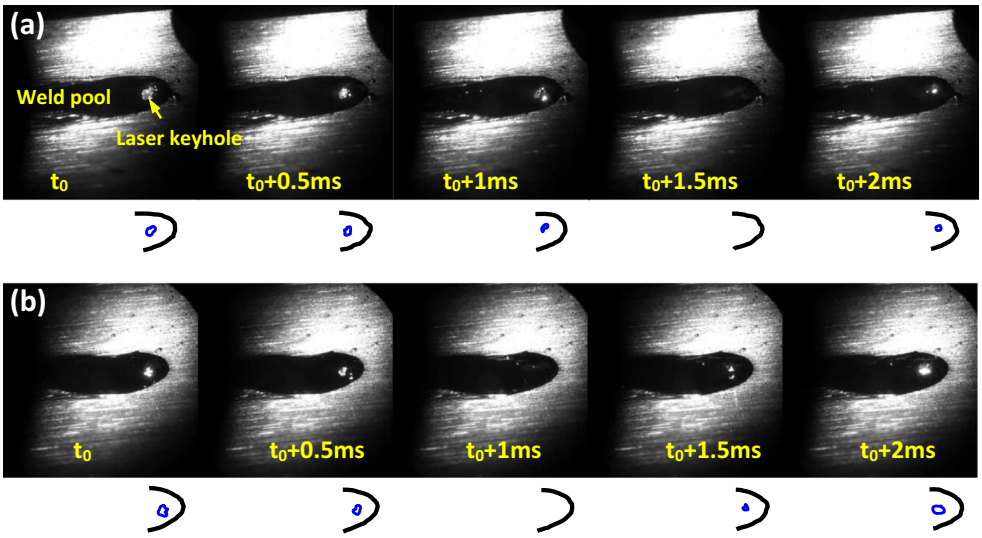


**Fig. 18** The keyhole behavior using a laser power of 10 kW, a welding speed of 0.8 m/min, and a shielding gas of **a** Ar and **b** $N_2$

periodically, as shown in Fig. 17f–h. The metallic plume produced with $N_2$ was also observed and the results are shown in Fig. 17i–l. Similar phenomenon about the variation of the plume was also found.

The melt pool and keyhole behavior were also observed, and the results are shown in Fig. 18. Every figure in Fig. 18 was obtained with an interval of 0.5 ms. Figure 18a presented the melt pool made in Ar. As seen, the shape and size of the laser keyhole was fluctuated drastically, which was caused by many factors such as the dynamic plasma variation and the strong liquid metal flow. At $t_0$ + 1.5 ms, the laser keyhole even disappeared due to the keyhole collapse. Figure 18b presented the melt pool made in $N_2$. The keyhole behavior was similar to that made in Ar, which also varied greatly. Occasional collapse of the keyhole was still observed.

Elmer et al. [19] thought it is not clear that one gas would have a distinct advantage over the other in terms of interacting with the laser plume or stabilizing the keyhole based on the physical properties of Ar and $N_2$ alone. Li et al. [21] found that nitrogen had little effect on the surface tension of liquid stainless steel. Therefore, $N_2$ did not contribute to the improvement of the keyhole stability during laser welding process, which was accordant to the laser keyhole behavior observed here.

The shielding gases of Ar and $N_2$ behaved similarly in terms of beam interaction and keyhole stabilization from the above analysis. Thus, it was speculated that the almost elimination of porosity in the laser welds made in $N_2$ gas must be related to the escape of the bubbles from the liquid weld pool or the dissolution of them into the weld metal. It can be seen from Fig. 8 a, b that a great mass of porosity was retained using Ar, and barely any bubble escaped from the weld pool according to Fig. 14a. So, assuming that both Ar and $N_2$ gases could not dissolve into the weld metal, it could be reasonably speculated that large amount of porosity would also be retained in the laser weld with $N_2$. However, Fig. 10a shows the porosity in the longitude section that was produced with the same condition to that of Fig. 8a except the shielding gas, but only few pores with small volume were observed. Therefore, the dissolution of the shielding gas into the weld pool was considered. The Ar is known to be an inert gas, which cannot react with the stainless or dissolve in the liquid weld pool. However, the nitrogen can dissolve in the stainless weld pool, and the solubility of $N_2$ in 304L stainless steel is 0.28 wt% [22]. Consequently, it was concluded that the elimination of the porosity was attributed to the dissolution of $N_2$ into the weld metal.

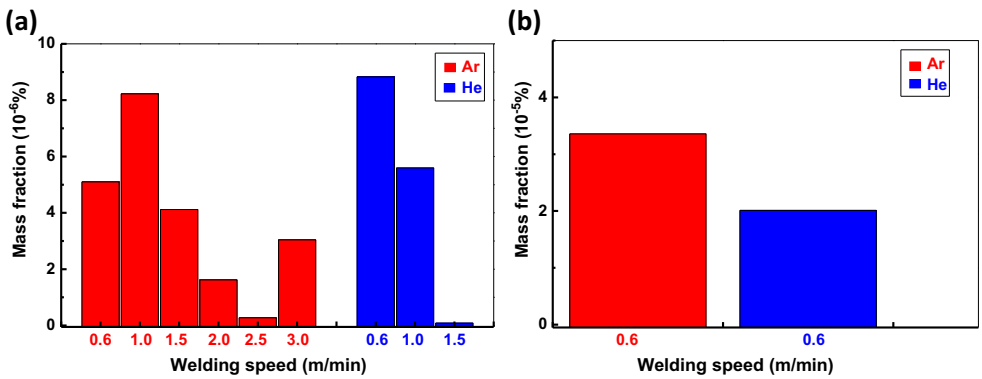


**Fig. 19** The equivalent nitrogen content for all the welds in Figs. 8 and 9 based on **a** the mean diameter $D_{mean}$ and **b** the maximum diameter $D_{max}$ of the porosity

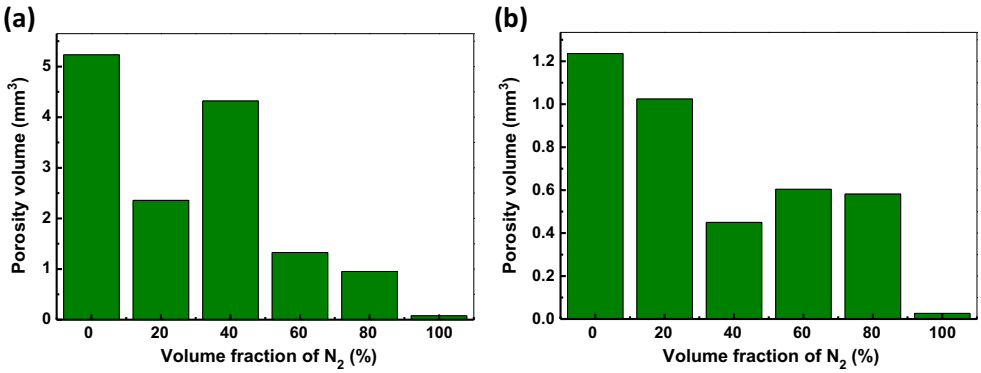


**Fig. 20** The total porosity volume in the laser welds with a length of 60 mm made in the mixed gases of Ar + $N_2$ in different proportion, at a laser power of 10 kW and a welding speed of **a** 0.6 and **b** 1.5 m/min

The porosity was formed in the welds using Ar and He. The quantitative estimates of the amount of porosity were conducted by the volume fraction of each weld. Assuming an equivalent amount of porosity was initially produced by $N_2$ in the welds due to keyhole instability, the increase of the nitrogen content in the liquid weld metal could be calculated by assuming that the weld metal had sufficient solubility of nitrogen, and all the $N_2$ porosity could be quickly dissolved into the liquid weld metal. According to this assumption, the increasing nitrogen content was calculated, and the results are shown in Fig. 19. Figure 19a was obtained according to the mean diameter $D_{mean}$ of the porosity, and Fig. 19b was obtained according to the maximum diameter $D_{max}$ of the porosity. The largest amount was $3.358 \times 10^{-5}$ wt.%, when a shielding gas of Ar and a welding speed of 0.6 m/min were used. If all the porosity was full of $N_2$ and it could completely dissolve into the liquid weld metal, the increase of the nitrogen content in weld metal was $3.358 \times 10^{-5}$ wt.%, which was far below the solubility limit of 0.28 wt%.

In order to further demonstrate that the reduction or elimination of porosity in the laser welds was attributed to the dissolution of $N_2$ into the liquid weld metal, the mixed gases of Ar + $N_2$ were applied as the shielding gas. The welding processes were conducted at a laser of 10 kW and different welding speeds of 0.6 and 1.5 m/min. The porosity volume in the laser welds with a length of 60 mm was measured, and the results are shown in Fig. 20. More porosity was produced in the laser welds in Fig. 20a, when a welding speed of 0.6 m/min was used, compared to that produced in the laser welds when a welding speed of 1.5 m/min was used (i.e., Fig. 20b). However, it was found that the porosity volume reduced, though occasional fluctuations occurred, with increasing $N_2$ content. Studies by Lai et al. [23] and Keskitalo et al. [24] also indicated that the nitrogen was absorbed by the stainless during the welding process. Therefore, it was confirmed that the solubility of $N_2$ played a significant role in reducing the porosity.

The formation and elimination of porosity in high-power laser welds was summarized, and the schematic of the welding process was illustrated in Fig. 21a–f. The welding process produced in the Ar gas is presented in Fig. 21a–c. As shown in Fig. 21b, e, the laser keyhole could collapse whatever

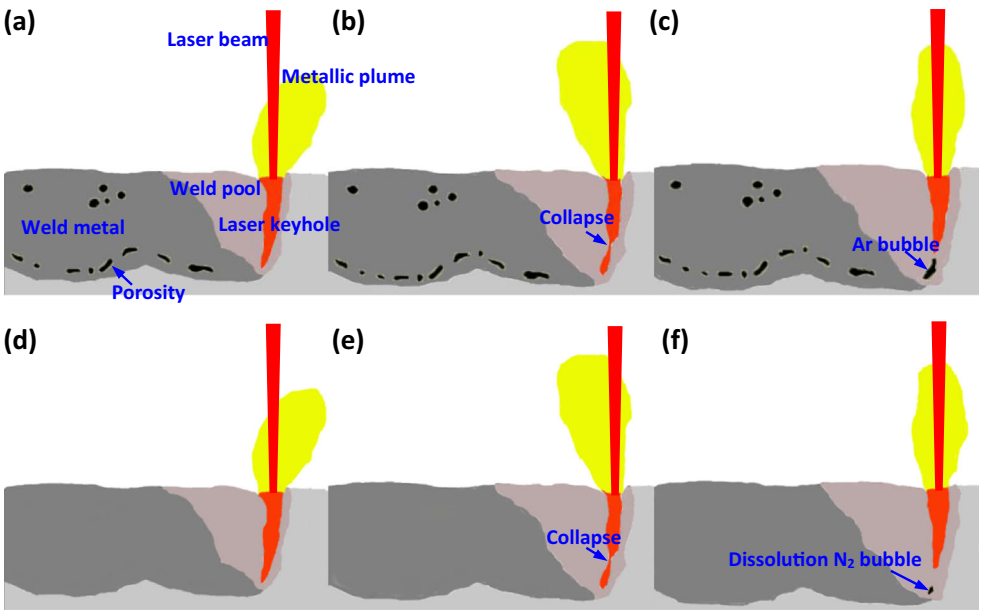


**Fig. 21** Schematic of the porosity formation using different shielding gas of **a**–**c** Ar and **d**–**f** $N_2$

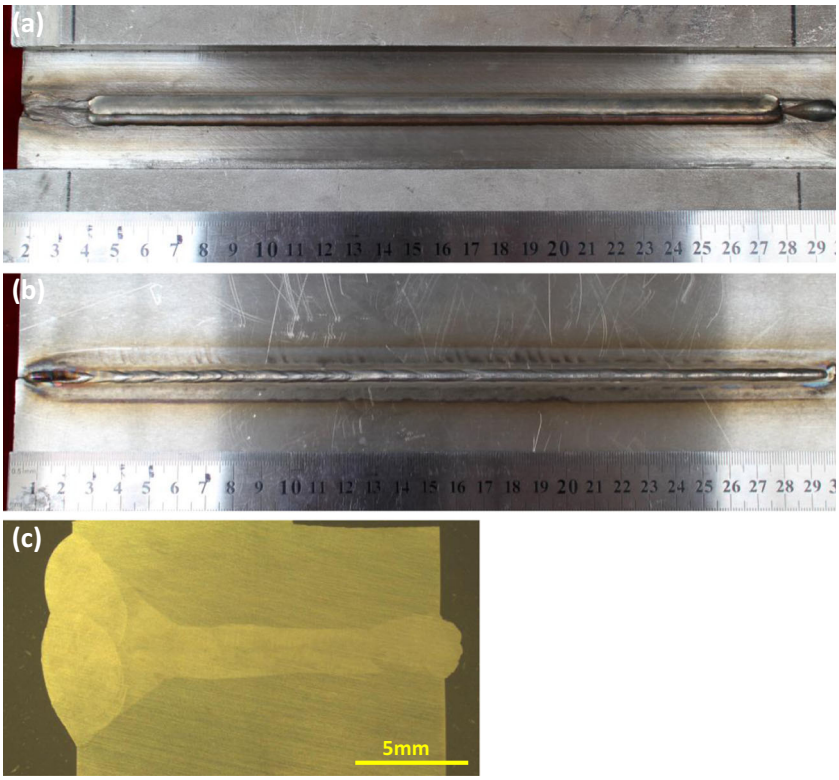


**Fig. 22** **a** The top appearance, **b** the bottom appearance, and **c** the cross-section of the laser weld using $N_2$ shielding gas

shielding gas was chosen. The bubbles, which included the shielding gas and the melt vapor, were created at the low part of the molten pool. A great mass of porosity was retained in the weld after solidification, as shown in Fig. 21c. However, the $N_2$ bubbles disappeared because they dissolved into the molten pool immediately after generation, as shown in Fig. 21f. Therefore, no porosity was found after welding.

### 3.5 Sound joint of laser welding of a thick 304L plate

A large specimen which had a length of 300 mm and a thickness of 16 mm was welded, and the result is shown in Fig. 22. An autogenous laser welding process was applied to join the thick plate with a square groove firstly. A laser power of 10 kW and a weld speed of 0.8 m/min were used. Then, laser welding assisted with a cold wire was used to fill the unfilled joint. A laser power of 4 kW, a wire feed rate of 2 m/min, and a weld speed of 0.42 m/min were used. As shown, both the top and bottom appearances were smooth and continuous. No significant porosity was examined in the weld by using the shielding gas of $N_2$.

## 4 Conclusion

1. Severe porosity was formed in the laser welds when Ar and He were used as the shielding gas during high-power laser welding of AISI 304L. The volume and the size of the porosity decreased with increasing welding speed. Almost no porosity was produced in the laser welds with $N_2$.
2. Most of the porosity was irregular, which mainly produced at the root due to keyhole collapse. A small quantity of porosity with spherical shape was found at the upper part of the weld. The statistics on the porosity size distribution the distributions revealed a decreasing frequency with increasing porosity volume, with the largest frequencies occurring at porosity less than 0.02 $mm^3$.
3. The behaviors of the metallic plume, the metal pool, and the laser keyhole were similar when different shielding gases of Ar and $N_2$ were used. The bubbles were produced for both cases because keyhole collapse was observed for Ar and $N_2$.
4. The solubility of the $N_2$ shielding gas with the liquid 304L melt pool resulted in the elimination of the gas bubbles, leading to no measurable porosity in the laser welds made in $N_2$ gas.
5. The specimen that has a length of 300 mm and a thickness of 16 mm is welded using fiber laser welding process, and sound joint without the porosity was obtained.

**Acknowledgements** The authors acknowledge funding from the Shuguang Project (No.12SG15) of Shanghai Municipal Education Committee, National Nature Science Foundation of China (No. 51675336 and No. 51505271), Shanghai No. 1 Machine Tool Works Co., Ltd., as well as the analysis support by Y.F. Gu, L.Z. Hong, and Z.Q. Bao of Instrumental Analysis Center at SJTU.

## References


1. Zhang M, Chen G, Zhou Y, Liao S (2014) Optimization of deep penetration laser welding of thick stainless steel with a 10 kW fiber laser. Mater Des 53:568–576
2. Shen X, Li L, Guo W, Teng W, He W (2016) Comparison of processing window and porosity distribution in laser welding of 10mm thick 30CrMnSiA ultrahigh strength between flat (1G) and horizontal (2G) positions. J Laser Appl 28:022418/1–022418/9
3. Atabaki M, Yazdian N, Ma J, Kovacevic R (2016) High power laser welding of thick steel plates in a horizontal butt joint configuration. Opt Laser Technol 83:1–12
4. Beretta S, Previtali B (2009) Estimate of maximum pore size in keyhole laser welding of carbon steel. Sci Technol Weld Join 14: 106–116
5. Tsukamoto S (2011) High speed imaging technique part 2-high speed imaging of power beam welding phenomena. Sci Technol Weld Join 16:44–55
6. Ola O, Doern F (2015) Keyhole-induced porosity in laser-arc hybrid welded aluminum. Int J Adv Manuf Technol 80:3–10
7. Matsunawa A (2001) Problems and solutions in deep penetration laser welding. Sci Technol Weld Join 6:351–354
8. Kawahito Y, Mizutani M, Katayama S (2009) High quality welding of stainless steel with 10 kW high power fiber laser. Sci Technol Weld Join 14:288–294
9. Zhao H, Niu W, Zhang B, Lei Y, Kodama M, Ishide T (2011) Modeling of keyhole dynamics and porosity formation considering the adaptive keyhole shape and three-phase coupling during deep-penetration laser welding. J Phys D Appl Phys 44:485302/1–485302/13
10. Kuo T, Jeng S (2005) Porosity reduction in Nd-YAG laser welding of stainless steel and inconel alloy by using a pulsed wave. J Phys D Appl Phys 38:722–728
11. Harooni M, Carlson B, Strohmeier B, Kovacevic R (2014) Pore formation mechanism and its mitigation in laser welding of AZ31B magnesium alloy in lap joint configuration. Mater Des 58: 265–276
12. Kamimuki K, Inoue T, Yasuda K, Muro M, Nakabayashi T, Matsunawa A (2002) Prevention of welding defect by side gas flow and its monitoring method in continuous wave Nd: YAG laser welding. J. Laser Appl. 14:136–145
13. Meng W, Li Z, Huang J, Wu Y, Katayama S (2014) The influence of various factors on the geometric profile of laser lap welded T-joints. Int J Adv Manuf Technol 74:1625–1636
14. Li K, Lu F, Cui H, Li X, Tang X, Li Z (2015) Investigation on the effects of shielding gas on porosity in fiber laser welding of T-joint steels. Int J Adv Manuf Technol 77:1881–1888
15. Sun J, Feng K, Zhang K, Guo B, Jiang E, Nie P, Li Z (2017) Fiber laser welding of thick AISI 304 plate in a horizontal (2G) butt joint configuration. Mater Des 118:53–65
16. Wei P, Chao T (2015) The effects of entrainment on pore shape in keyhole mode welding. J Heat Trans 137:082102/1–082102/9
17. Tucker J, Nolan T, Martin A, Young G (2012) Effect of travel speed and beam focus on porosity in alloy 690 laser welds. J Miner Met Mater Soc (JOM) 64:1409–1417
18. Katayama S, Mizutani M, Matsunawa A (2003) Development of porosity prevention procedures during laser welding. Proc SPIE 4331:281–288
19. Elmer J, Vaja J, Carlton H, Pong R (2015) The effect of Ar and $N_2$ shielding gas on laser weld porosity in steel, stainless steels, and nickel. Weld J 94:313–325
20. Pang S, Chen X, Shao X, Gong S, Xiao J (2016) Dynamics of vapor plume in transient keyhole during laser welding of stainless steel: local evaporation, plume swing and gas entrapment into porosity. Opt Laser Technol 82:28–40
21. Li Z, Mukai K, Zeze M, Mills K (2005) Determination of the surface tension of liquid stainless steel. J Mater Sci 40:2191–2195
22. Dischino A, Kenny J, Mecozzi M, Barteri M (2000) Development of high nitrogen, low nickel, 18%Cr austenitic stainless steels. J Mater Sci 35:43803–43808
23. Lai R, Cai Y, Wu Y, Li F, Hua X (2016) Influence of absorbed nitrogen on microstructure and corrosion resistance of 2205 duplex stainless steel joint processed by fiber laser welding. J Mater Process Tech 231:397–405
24. Keskitalo M, Mantyjarvi K, Sundqvist J, Powell J, Kaplan A (2016) Laser welding of duplex stainless steel with nitrogen as shielding gas. J Mater Process Tech 216:381–384